

Synthesis and reactivity of (μ - η^2 : η^2 -peroxo)dicopper(II) complexes with dinucleating ligands: Hydroxylation of xylyl linker with a NIH shift

Takahiro Matsumoto^a, Hideki Furutachi^a, Shigenori Nagatomo^b, Takehiko Tosha^b,
Shuhei Fujinami^a, Teizo Kitagawa^b, Masatatsu Suzuki^{a,*}

^a Department of Chemistry, Graduate School of Natural Science and Technology, Kanazawa University, Kakuma-machi, Kanazawa 920-1192, Japan

^b Center for Integrative Bioscience, Okazaki National Research Institutes, Myodaiji, Okazaki 444-8585, Japan

Received 16 March 2006; received in revised form 3 May 2006; accepted 12 May 2006

Available online 9 September 2006

Abstract

New hexadentate dinucleating ligands having a xylyl linker, X–L–R, were synthesized, where X–L–R = 1,3-bis[bis(6-methyl-2-pyridylmethyl)aminomethyl]-2,4,6-trimethylbenzene (Me₂–L–Me) and 1,3-bis[bis(6-methyl-2-pyridylmethyl)aminomethyl]-2-fluorobenzene (H–L–F). They form dinuclear copper(I) complexes, [Cu₂(X–L–R)]²⁺ (Me₂–L–Me (**1**) and H–L–F (**2**)). The copper(I) complexes in acetone at –78 °C react with O₂ to produce intra- and intermolecular (μ - η^2 : η^2 -peroxo)dicopper(II) species depending on the concentrations of the complexes: both complexes generate intramolecular (μ - η^2 : η^2 -peroxo)dicopper(II) species [Cu₂(O₂)(X–L–R)]²⁺ (**1**-O₂ and **2**-O₂) at the concentrations below ~5 mM, whereas at ~60 mM, both complexes produce intermolecular (μ - η^2 : η^2 -peroxo)dicopper(II) species, which were confirmed by the electronic and resonance Raman spectroscopies. The electronic spectrum of **1**-O₂ in acetone at concentrations below ~5 mM showed an absorption band at ($\lambda_{\text{max}} = 442 \text{ nm}$, $\epsilon = 5600 \text{ M}^{-1} \text{ cm}^{-1}$) assignable to the $\pi_{\sigma}^*(\text{O}-\text{O})$ -to-Cu(II) ($(d_{x^2-y^2} + d_{z^2-y^2})$ component) LMCT transition in addition to an intense band attributable to the $\pi_{\sigma}^*(\text{O}-\text{O})$ -to-Cu(II) ($(d_{x^2-y^2} - d_{z^2-y^2})$ component) LMCT transition ($\lambda_{\text{max}} = 359 \text{ nm}$, $\epsilon = 21000 \text{ M}^{-1} \text{ cm}^{-1}$), indicating that the (μ - η^2 : η^2 -peroxo)Cu(II)₂ core of **1**-O₂ takes a butterfly structure. Decomposition of **1**-O₂ resulted in hydroxylation of the 2-position of the xylyl linker with 1,2-methyl migration (NIH shift), suggesting that the hydroxylation reaction proceeds via a cationic intermediate as proposed for closely related (μ - η^2 : η^2 -peroxo)Cu(II)₂ complexes having a xylyl linker. Kinetic study of the decomposition (hydroxylation of the xylyl linker) of **1**-O₂ suggests that a stereochemical effect of the methyl group in the 2-position of the xylyl linker has a significant influence on a transition state for decomposition (hydroxylation of the xylyl linker).

© 2006 Elsevier B.V. All rights reserved.

Keywords: Dinuclear copper complexes; Arene hydroxylation; Oxygenation; Peroxo dicopper complexes

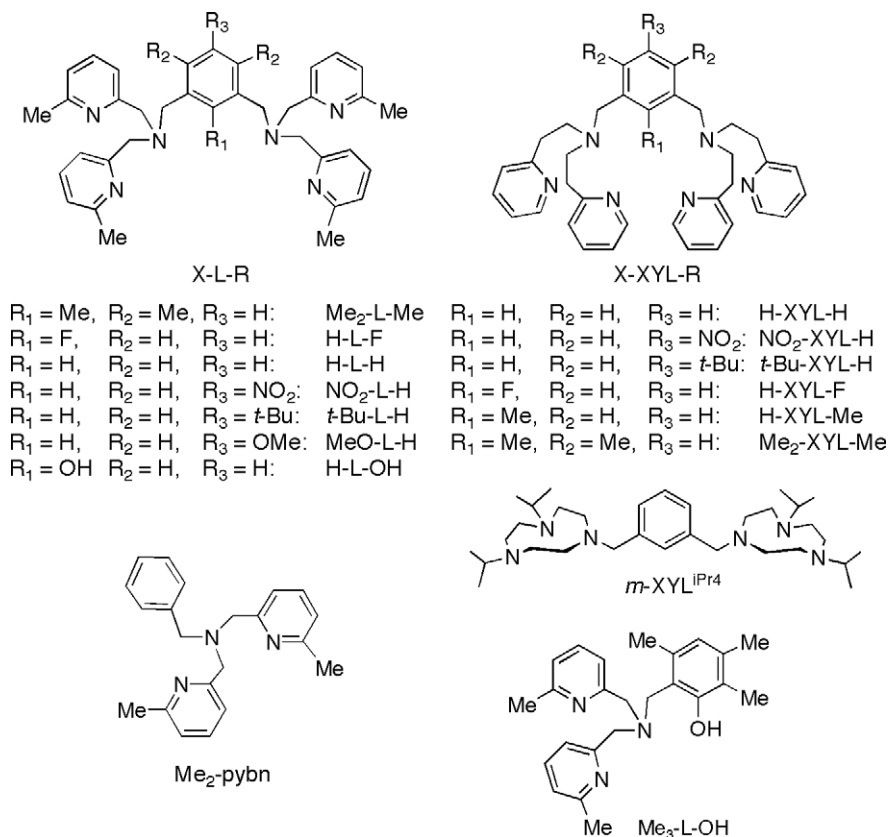
1. Introduction

The Cu_n/O₂-mediated arene hydroxylation is of current interest for understanding the reaction mechanisms of dioxygen activating copper proteins in biological systems such as tyrosinase and utilizing metal complexes as oxidation catalysts [1–15]. Karlin and co-workers have first demonstrated that the (μ - η^2 : η^2 -peroxo)Cu(II)₂ complexes, [Cu₂(O₂)(X–XYL–R)]²⁺, are capable of performing

hydroxylation of the xylyl linkers of the supporting ligands [3–5]. The detailed kinetic studies of the decompositions of [Cu₂(O₂)(X–XYL–H)]²⁺ (X = NO₂, H, and *t*-Bu, see Scheme 1) have revealed that Hammett ρ value is –2.1, suggesting that the hydroxylation mediated by [Cu₂(O₂)(X–XYL–H)]²⁺ proceeds via an electrophilic aromatic substitution mechanism [6]. In addition to such intramolecular reactions, intermolecular arene hydroxylation reactions have also been demonstrated where phenolates are hydroxylated by the (μ - η^2 : η^2 -peroxo)Cu(II)₂ complexes [8–11]. Itoh and co-workers have shown that the phenolate hydroxylation by a (μ - η^2 : η^2 -peroxo)copper(II) complex

* Corresponding author. Fax: +81 76 264 5742.

E-mail address: suzuki@cacheibm.s.kanazawa-u.ac.jp (M. Suzuki).



Scheme 1.

well mimics that performed by tyrosinase [9,12]. Recently, we have also found that a $(\mu\text{-}\eta^2\text{:}\eta^2\text{-peroxo})\text{Cu}(\text{II})_2$ having a xylyl linker $[\text{Cu}_2(\text{O}_2)(\text{H-L-H})]^{2+}$ (**3-O₂**) is capable of performing not only intramolecular hydroxylation of the xylyl linker of the dinucleating ligand H-L-H, but also intermolecular epoxidation of styrene and hydroxylation of THF by hydrogen atom abstraction [13].

It has been shown that a bis($\mu\text{-oxo}$)Cu(III)₂ species is also capable of hydroxylation of phenyl group of a supporting ligand via an electrophilic aromatic substitution mechanism [14]. Recently, Stack and co-workers also have reported intermolecular hydroxylation reaction of phenolates by a bis($\mu\text{-oxo}$)Cu(III)₂ species, where coordination of a phenolate to a $(\mu\text{-}\eta^2\text{:}\eta^2\text{-peroxo})\text{Cu}(\text{II})_2$ species causes the O-O bond cleavage to generate a bis($\mu\text{-oxo}$)Cu(III)₂ species which is responsible for the hydroxylation of a phenolate via an electrophilic aromatic substitution mechanism [15]. Thus, these model studies have provided chemical insights into the arene hydroxylation reactions performed by both $(\mu\text{-}\eta^2\text{:}\eta^2\text{-peroxo})\text{Cu}(\text{II})_2$ and bis($\mu\text{-oxo}$)Cu(III)₂ species.

Reaction of dinuclear copper(I) complexes $[\text{Cu}_2(\text{Me}_2\text{-XYL-Me})]^{2+}$ and $[\text{Cu}_2(\text{H-XYL-Me})]^{2+}$ with O₂ has been shown to cause the hydroxylation at the 2-position of the xylyl linker with a 1,2-migration of the methyl group (NIH shift) involving the elimination of a bis(pyridylethyl) aminomethyl group from the supporting ligand, support-

ing that the hydroxylation proceeds via an electrophilic pathway involving a carbocationic intermediate [4]. However, in the above oxidation reaction, no $(\mu\text{-}\eta^2\text{:}\eta^2\text{-peroxo})\text{Cu}(\text{II})_2$ species has been identified. So, it is important to definitively confirm the presence of a $(\mu\text{-}\eta^2\text{:}\eta^2\text{-peroxo})\text{Cu}(\text{II})_2$ species as a reaction intermediate and, if present, to know the nature of $(\mu\text{-}\eta^2\text{:}\eta^2\text{-peroxo})\text{Cu}(\text{II})_2$ species, since the methyl group in the 2-position of a xylyl linker could have significant influence on the stereochemistry and electronic nature of $(\mu\text{-}\eta^2\text{:}\eta^2\text{-peroxo})\text{Cu}(\text{II})_2$ species. Recently, we found that the $(\mu\text{-}\eta^2\text{:}\eta^2\text{-peroxo})\text{Cu}(\text{II})_2$ species $[\text{Cu}_2(\text{O}_2)(\text{H-L-H})]^{2+}$ (**3-O₂**) is 100 times stable compared to $[\text{Cu}_2(\text{O}_2)(\text{H-XYL-H})]^{2+}$ (**6-O₂**), which allowed us to observe **3-O₂** by benchtop UV-Vis monitoring.

In order to investigate physicochemical properties of a $(\mu\text{-}\eta^2\text{:}\eta^2\text{-peroxo})\text{Cu}(\text{II})_2$ species which has a methyl or a fluorine in the 2-position of xylyl linker, we prepared new dinucleating ligands, Me₂-L-Me and H-L-F shown in Scheme 1, and their dinuclear copper(I) complexes, $[\text{Cu}_2(\text{Me}_2\text{-L-Me})]^{2+}$ (**1**) and $[\text{Cu}_2(\text{H-L-F})]^{2+}$ (**2**). The complexes produce $(\mu\text{-}\eta^2\text{:}\eta^2\text{-peroxo})\text{Cu}(\text{II})_2$ species, $[\text{Cu}_2(\text{O}_2)(\text{Me}_2\text{-L-Me})]^{2+}$ (**1-O₂**) and $[\text{Cu}_2(\text{O}_2)(\text{H-L-F})]^{2+}$ (**2-O₂**), which were characterized by resonance Raman and UV-Vis spectroscopies. Decomposition of **1-O₂** resulted in hydroxylation of the xylyl linker of Me₂-L-Me with a 1,2-migration of the methyl group (NIH shift)

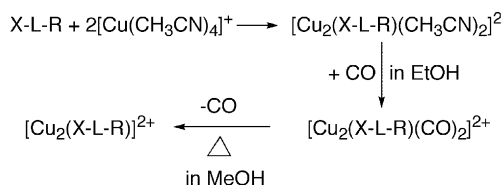
to produce dinuclear $[\text{Cu}_2(\text{Me}_2\text{-L-O})_2]^{2+}$ (**4**). Kinetic study of the decompositions of **1-O**₂ and **2-O**₂ is also described.

2. Results and discussion

2.1. Synthesis and characterization of copper(I) complexes

Copper(I) complexes, $[\text{Cu}_2(\text{X-L-R})(\text{CH}_3\text{CN})_2]^{2+}$ ($\text{X-L-R} = \text{Me}_2\text{-L-Me}$ (**1-CH**₃CN) and H-L-F (**2-CH**₃CN)), were prepared as yellow–green powders by the reaction of $[\text{Cu}(\text{CH}_3\text{CN})_4]^+$ with the dinucleating ligands in acetonitrile/ethanol/water mixture under N_2 as in the case of $[\text{Cu}_2(\text{H-L-H})(\text{CH}_3\text{CN})_2]^{2+}$ (**3-CH**₃CN) [13]. Solid samples are relatively stable against O_2 and can be handled in air. Crystal structure of **1a-CH**₃CN shows that each Cu(I) site has a tetrahedral structure with two pyridyl nitrogens, one tertiary amine nitrogen, and an additional CH_3CN as shown in Fig. 1. The $\text{Cu}\cdots\text{Cu}$ distance is 8.995 Å, which is comparable to that of $[\text{Cu}_2(\text{H-XYL-H})]^{2+}$ (**6**) (8.940 Å) [3] and shorter than that of $[\text{Cu}_2(m\text{-XYL}^{i\text{Pr}4})(\text{CO})_2]^{2+}$ (**7-CO**, 10.061 Å) [7]. H-XYL-H forms a tri-coordinate complex, whereas $m\text{-XYL}^{i\text{Pr}4}$ and X-L-R form four-coordinate complexes with an additional CH_3CN . However, dioxygen reactivities of **7-CH**₃CN and $[\text{Cu}_2(\text{X-L-R})(\text{CH}_3\text{CN})_2]^{2+}$ significantly differ; oxygenation of **1-CH**₃CN, **2-CH**₃CN, and **3-CH**₃CN is very slow and not fully completed probably due to strong coordination of CH_3CN , whereas **7-CH**₃CN is readily oxygenated [7]. Thus, for full oxygenation, we prepared $[\text{Cu}_2(\text{X-L-R})]^{2+}$ (**1**, **2**, and **3**) from $[\text{Cu}_2(\text{X-L-R})(\text{CH}_3\text{CN})_2]^{2+}$ through $[\text{Cu}_2(\text{X-L-R})(\text{CO})_2]^{2+}$. Reaction of $[\text{Cu}_2(\text{X-L-R})(\text{CH}_3\text{CN})_2]^{2+}$ in ethanol with CO gave corresponding carbonyl complexes, $[\text{Cu}_2(\text{X-L-R})(\text{CO})_2]^{2+}$ (**1-CO**, **2-CO**, and **3-CO**). The IR spectra of the complexes showed strong

$\nu(\text{C-O})$ bands at 2096 and 2085 cm^{-1} for **1-CO**, 2089 cm^{-1} for **2-CO**, and 2092 cm^{-1} for **3-CO**, which are comparable to those of $[\text{Cu}(\text{Me}_2\text{-pybn})(\text{CO})]^{2+}$ (**5-CO**, 2100 and 2088 cm^{-1}) that has a half part of the dinucleating ligand H-L-H (see Scheme 1) [16] and **7-CO** (2079 cm^{-1}) [7], indicating that the electron donor properties of these mono- and dinucleating ligands are similar [7,16,17]. The coordinated CO ligands in $[\text{Cu}_2(\text{X-L-R})(\text{CO})_2]^{2+}$ can be removed by refluxing the methanol solutions under N_2 to afford $[\text{Cu}_2(\text{X-L-R})]^{2+}$ (**1**, **2**, and **3**) as air-sensitive yellow powders.



2.2. Spectroscopic characterization of $(\mu\text{-}\eta^2\text{:}\eta^2\text{-peroxo})\text{Cu}(\text{II})_2$ complexes

The copper(I) complexes **1**, **2**, and **3** in acetone at -78°C react with O_2 to produce the brown $(\mu\text{-}\eta^2\text{:}\eta^2\text{-peroxo})\text{dicopper}(\text{II})$ complexes, $[\text{Cu}_2(\text{O}_2)(\text{X-L-R})]^{2+}$ (**1-O**₂ ($\text{Me}_2\text{-L-Me}$), **2-O**₂ (H-L-F), and **3-O**₂ (H-L-H)), which were characterized by resonance Raman and electronic spectroscopies. It has been shown that the oxygenation of the dicopper(I) complexes having a xylyl linker such as $[\text{Cu}_2(\text{NO}_2\text{-XYL-H})]^{2+}$ (**NO**₂-**6**) and $[\text{Cu}_2(m\text{-XYL}^{i\text{Pr}4})]^{2+}$ (**7**) generate both intramolecular $(\mu\text{-}\eta^2\text{:}\eta^2\text{-peroxo})\text{Cu}(\text{II})_2$ species and intermolecular $(\mu\text{-}\eta^2\text{:}\eta^2\text{-peroxo})\text{Cu}(\text{II})_2$ or bis($\mu\text{-oxo})\text{Cu}(\text{III})_2$ species such as a dimer depending on the concentrations of the complexes and the nature of the side arms [5,7]. **NO**₂-**6** generates an intramolecular $(\mu\text{-}\eta^2\text{:}\eta^2\text{-peroxo})\text{Cu}(\text{II})_2$ species at the concentrations below 4 mM, whereas **7** generates an intermolecular bis($\mu\text{-oxo})\text{Cu}(\text{III})_2$ species even at the concentration of 0.1 mM. Thus the formation of intramolecular and intermolecular species are highly dependent on not only the concentration of complex, but also the nature of the side arm of the dinucleating ligand. Similar observation was also made for the present complexes.

The resonance Raman spectra of **1-O**₂ and **3-O**₂ in acetone (~ 5 mM) measured with a 406.7 nm laser excitation show isotope-sensitive bands at 752 cm^{-1} ($^{16-18}\Delta = 42$) (Fig. 2) and 744 cm^{-1} ($^{16-18}\Delta = 40$) [13], respectively, which are typical of the $\nu(\text{O-O})$ of the $(\mu\text{-}\eta^2\text{:}\eta^2\text{-peroxo})\text{Cu}(\text{II})_2$ complexes and no $\nu(\text{Cu-O})$ band in the 550–630 cm^{-1} region attributable to the bis($\mu\text{-oxo})\text{Cu}(\text{III})_2$ species is observed [18,19]. However, the spectrum of **2-O**₂ is quite different from those of **1-O**₂ and **3-O**₂; the spectrum shows two isotope sensitive bands at 744 cm^{-1} ($^{16-18}\Delta = 38$) and 726 cm^{-1} ($^{16-18}\Delta = 38$) in the $\nu(\text{O-O})$ region, and some isotope sensitive features in the 550–600 cm^{-1} region (the $\nu(\text{Cu-O})$ region). The two bands at 744 and 726 cm^{-1} suggest the presence of two types of $(\mu\text{-}\eta^2\text{:}\eta^2\text{-peroxo})\text{Cu}(\text{II})_2$

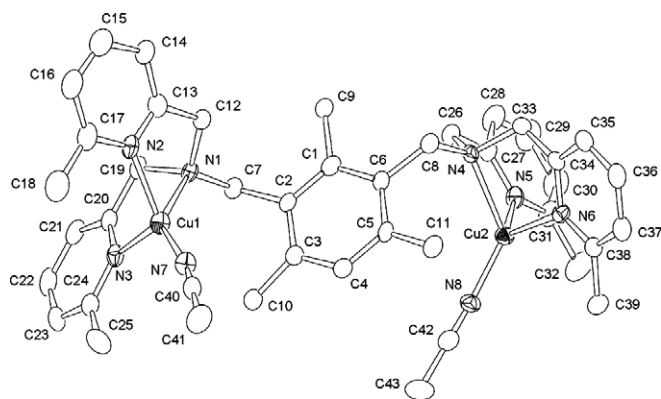


Fig. 1. ORTEP view (50% probability) of the cation of $[\text{Cu}_2(\text{Me}_2\text{-L-Me})(\text{CH}_3\text{CN})_2](\text{PF}_6)_2 \cdot 0.5\text{CH}_3\text{CN} \cdot 0.25\text{H}_2\text{O}$ (**1a-CH**₃CN). Hydrogen atoms are omitted for clarity. Selected bond distances (Å) and angles ($^\circ$): $\text{Cu1}\cdots\text{Cu2}$ 8.995(1), Cu1-N1 2.233(5), Cu1-N2 2.069(5), Cu1-N3 2.044(5), Cu1-N7 1.906(5), Cu2-N4 2.251(4), Cu2-N5 2.007(5), Cu2-N6 2.063(5), Cu2-N8 1.893(5), N1-Cu1-N2 77.8(2), N1-Cu1-N3 80.2(2), N1-Cu1-N7 141.5(2), N2-Cu1-N3 110.0(2), N2-Cu1-N7 113.8(2), N3-Cu1-N7 124.0(2), N4-Cu2-N5 80.9(2), N4-Cu2-N6 81.4(2), N4-Cu2-N8 125.8(2), N5-Cu2-N6 113.4(2), N5-Cu2-N8 127.1(2), N6-Cu2-N8 115.2(2).

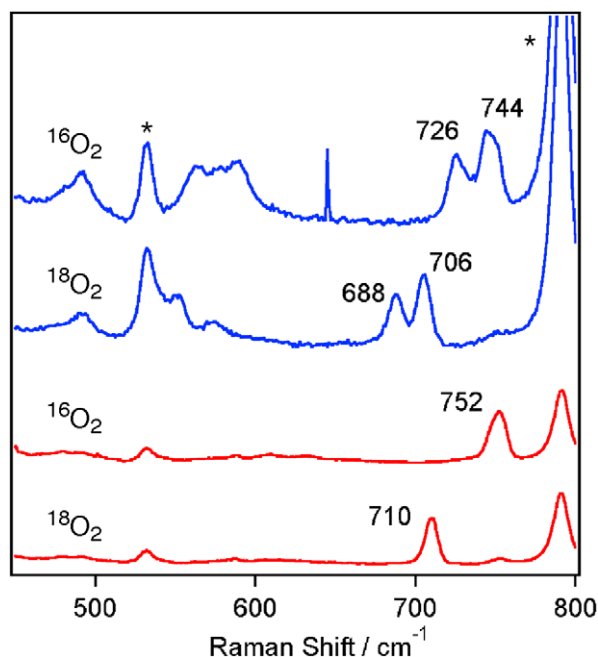


Fig. 2. Resonance Raman spectra of **1-O₂** (red) and **2-O₂** (blue) (~5 mM) in acetone at $-90\text{ }^{\circ}\text{C}$ measured with a 406.7 nm laser excitation. Asterisks are the solvent bands. (For interpretation of the references in colour in this figure legend, the reader is referred to the web version of this article.)

species, since $^{18}\text{O}_2$ sample also showed the two corresponding bands. The features in the $550\text{--}600\text{ cm}^{-1}$ region suggests a possibility of the presence of a bis(μ -oxo)Cu(III)₂ species (vide infra) [18,19]. It has been shown that the bands in the $550\text{--}600\text{ cm}^{-1}$ region attributable to the bis(μ -oxo)Cu(III)₂ species are unusually strongly enhanced by $\sim 400\text{ nm}$ laser excitation. Thus, the concentration of the bis(μ -oxo)Cu(III)₂ species, if present, seems to be low.

The resonance Raman spectra of the concentrated acetone solutions ($\sim 60\text{ mM}$) of **1-O₂**, **2-O₂**, and **3-O₂** measured with a 514.5 nm laser excitation showed new bands at 719, 714, and 715 cm^{-1} , respectively, as shown in Fig. 3. For **1-O₂** and **3-O₂**, the spectra also exhibit the bands at 752 and 745 cm^{-1} observed for the 5 mM samples, indicating that the bands at 719 and 714 cm^{-1} , and the bands at 752 and 745 cm^{-1} are attributable to those of the intermolecular and intramolecular (μ - η^2 : η^2 -peroxo)Cu(II)₂ species, respectively. It is noted that the $\nu(\text{O-O})$ of $[\text{Cu}_2(\text{O}_2)(\text{Me}_2\text{-pybn})_2]^{2+}$ (**5-O₂**) is observed at 714 cm^{-1} [16], which is almost the same as those of the present intermolecular (μ - η^2 : η^2 -peroxo)Cu(II)₂ species. Thus, the xylyl bridges of **1-O₂** and **3-O₂** have a substantial influence on the $\nu(\text{O-O})$ frequency. Such low $\nu(\text{O-O})$ frequency shifts in the intermolecular (μ - η^2 : η^2 -peroxo)Cu(II)₂ species may be partly attributable to the decrease of a donation from π_v^* orbital of the peroxo ligand to $4p_x$ orbital of the copper(II) compared to those of the intramolecular (μ - η^2 : η^2 -peroxo)Cu(II)₂ species which have a butterfly structure (vide infra) [20]. A similar lower frequency shift of the $\nu(\text{O-O})$ band of the intermolecular (μ - η^2 : η^2 -peroxo)-

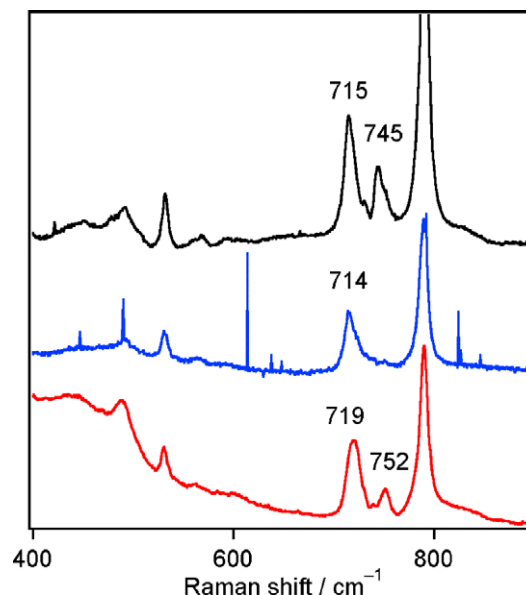


Fig. 3. Resonance Raman spectra of **1-O₂** (red), **2-O₂** (blue), and **3-O₂** (black) ($\sim 60\text{ mM}$) in acetone at $-90\text{ }^{\circ}\text{C}$ measured with a 514.5 nm laser excitation. Asterisks are the solvent bands. (For interpretation of the references in colour in this figure legend, the reader is referred to the web version of this article.)

Cu(II)₂ species of $[\text{Cu}_2(\text{O}_2)(\text{NO}_2\text{-XYL-H})]^{2+}$ (**NO₂-6-O₂**) has also been reported, although the shift (14 cm^{-1} (from 747 to 733 cm^{-1})) is significantly smaller than those of the present complexes [5]. Unlike **1-O₂** and **3-O₂**, **2-O₂** showed only a single band at 714 cm^{-1} attributable to an intermolecular (μ - η^2 : η^2 -peroxo)Cu(II)₂ species. It has been reported that $[\text{Cu}_2(\text{H-XYL-F})]^{2+}$ generates only an intermolecular (μ - η^2 : η^2 -peroxo)Cu(II)₂ species even at 4 mM [5]. Thus, introduction of the fluoro group into the xylyl linker tends to produce intermolecular (μ - η^2 : η^2 -peroxo)-Cu(II)₂ species, although the origin of this tendency is not known at present.

It is noted that the dilution of the 60 mM solution of **3-O₂** in acetone to 10 mM causes no significant change in the relative intensities of the $\nu(\text{O-O})$ bands at 715 and 744 cm^{-1} for 30 min at $-90\text{ }^{\circ}\text{C}$ as shown in Fig. 4, implying that the conversion between intramolecular and intermolecular (μ - η^2 : η^2 -peroxo) species is slow under the conditions. A similar behavior was also observed in the electronic spectra of **1-O₂**, **2-O₂**, and **3-O₂** (vide infra).

The electronic spectra of **1-O₂**, **2-O₂**, and **3-O₂** in acetone at $-80\text{ }^{\circ}\text{C}$ showed intense $\pi_v^*(\text{O-O})$ -to-Cu(II) ($(d_{x^2-y^2} - d_{z^2-y^2})$ component) LMCT bands ($\lambda_{\text{max}}/\text{nm}$ ($\epsilon/\text{M}^{-1}\text{ cm}^{-1}$)) at 359 (21000), 353 (26000), and 351 (32000) [13], respectively, which are characteristic of those of the (μ - η^2 : η^2 -peroxo)Cu(II)₂ complexes (Fig. 5a). The intensity of the LMCT transition decreases as the transition energy decreases, which seem to be closely related to the bulkiness of the substituents (F and CH₃) in the bridging xylyl linkers. The electronic spectra of **1-O₂** and **2-O₂** also showed additional bands at 442 nm ($\epsilon = 5600\text{ M}^{-1}\text{ cm}^{-1}$) and 433 nm ($\epsilon = 3400\text{ M}^{-1}\text{ cm}^{-1}$), respectively. Gaussian analysis

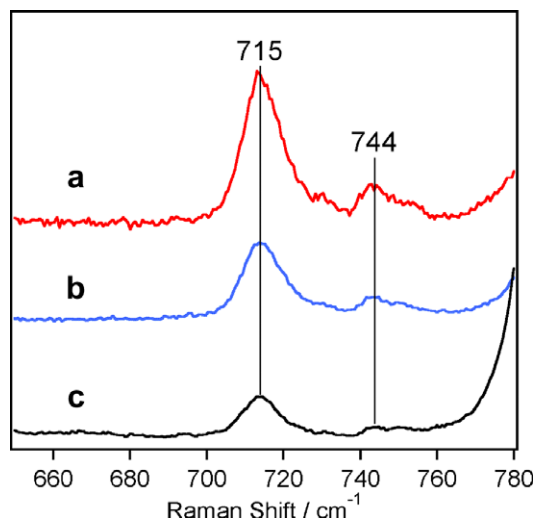
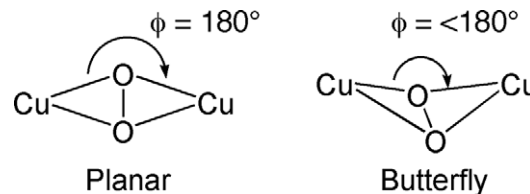


Fig. 4. Resonance Raman spectra of **3-O₂** at (a) ~60 mM (red), (b) ~30 mM (blue), and (c) ~10 mM (black) in acetone at $-90\text{ }^{\circ}\text{C}$ measured with a 514.5 nm laser excitation, where the samples of (b) and (c) were prepared by dilution of a 60 mM solution (a) (see text). (For interpretation of the references in colour in this figure legend, the reader is referred to the web version of this article.)

of the electronic spectrum of **3-O₂** revealed that **3-O₂** also has an additional band at ~390 nm. Similar spectral features have also been reported for $[\text{Cu}_2(\text{O}_2)(\text{NnPY}2)]^{2+}$ ($n = 3\text{--}5$) [20]. The additional absorption bands for **1-O₂** and **3-O₂** can be assigned to the $\pi^*(\text{O}\text{--}\text{O})\text{--}\text{to}\text{--}\text{Cu}(\text{II})$ ($(d_{x^2-y^2} + d_{x^2-y^2})$ component) LMCT transition based on the assignment made by Solomon et al. [20]. This transition has been shown to be forbidden for $(\mu\text{--}\eta^2:\eta^2\text{--}\text{peroxo})\text{--}\text{Cu}(\text{II})_2$ complex in a planar structure (C_{2h}), whereas the transition become allowed by a symmetry lowering (C_{2v}). Thus, the electronic spectra suggest that **1-O₂** and **3-O₂** also



Scheme 2.

have a butterfly structure. The intensity and transition energy of the forbidden band has been shown to be dependent on the bending of the Cu_2O_2 plane; as the angle ϕ shown in Scheme 2 becomes smaller, the intensity increases and the transition energy lowers. Thus, the order of the angles ϕ is **1-O₂** < **3-O₂**. This is also supported by the trend observed for the $\nu(\text{O}\text{--}\text{O})$ frequencies (752 cm^{-1} for **1-O₂** and 744 cm^{-1} for **3-O₂**). Solomon et al. reported that the $\nu(\text{O}\text{--}\text{O})$ is dependent on the magnitude of the angle ϕ of the butterfly core: a smaller angle ϕ causes a high frequency shift of the $\nu(\text{O}\text{--}\text{O})$, since the bending increases a donation from π^*_v orbital of the peroxo ligand to $4p_x$ orbital of the copper(II) [20]. Although the electronic spectrum of **2-O₂** shows a similar additional absorption band at 433 nm ($\epsilon = 3400\text{ M}^{-1}\text{ cm}^{-1}$) as noted earlier, there is a possibility of the presence of bis($\mu\text{--}\text{oxo}$) $\text{Cu}(\text{III})_2$ species which also has a LMCT band in this region. Further study is needed for fuller understanding of the spectroscopic properties of **2-O₂**.

It is noted that the intensities of the absorption bands observed at ~390–442 nm for the acetone solutions (~0.5 mM) of **1-O₂**, **2-O₂**, and **3-O₂** prepared by dilution of the 60 mM solutions decrease as shown in Fig. 5b, suggesting that the intermolecular $(\mu\text{--}\eta^2:\eta^2\text{--}\text{peroxo})\text{Cu}(\text{II})_2$ species have a planar structure.

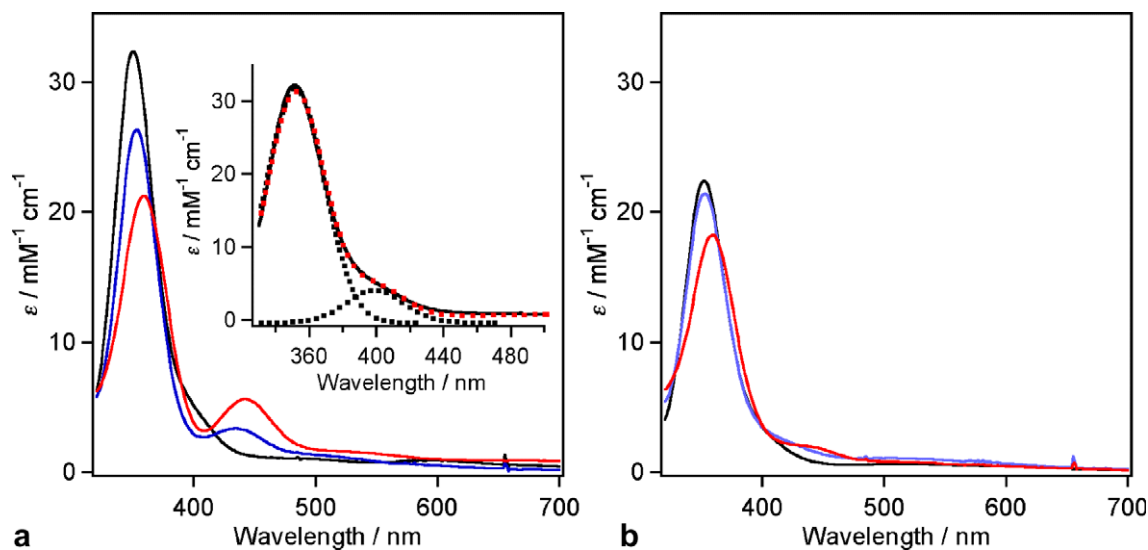


Fig. 5. (a) Electronic spectra of **1-O₂** (0.254 mM, red), **2-O₂** (0.265 mM, blue), and **3-O₂** (0.255 mM, black) in acetone at $-90\text{ }^{\circ}\text{C}$. Inset: Gaussian analysis of the spectrum of **3-O₂**. (b) Electronic spectra of **1-O₂** (0.5 mM, red), **2-O₂** (0.5 mM, blue), and **3-O₂** (0.5 mM, black) in acetone diluted from 60 mM acetone solutions at $-90\text{ }^{\circ}\text{C}$. Decrease of the intensities of the ~350 nm bands appear to be due to some decomposition during dilution processes. (For interpretation of the references in colour in this figure legend, the reader is referred to the web version of this article.)

2.3. Self-decompositions

Self decomposition of $[\text{Cu}_2(\text{O}_2)(\text{H-L-H})]^{2+}$ (3-O_2) in acetone ($< \sim 5$ mM) causes almost quantitative hydroxylation of the xylyl linker of H-L-H via an electrophilic aromatic substitution reaction [13]. However, decomposition of 3-O_2 in a concentrated acetone solution (~ 60 mM) at -60 °C which contains intra- and intermolecular ($\mu\text{-}\eta^2\text{:}\eta^2\text{-peroxo}$) species gave a hydroxylated ligand H-L-OH ($\sim 44\%$ yield based on 3-O_2) together with H-L-H ($\sim 38\%$), a ligand-based alcohol ($\sim 7\%$), and a ligand-based aldehyde ($\sim 9\%$). In the latter two modified ligands, one of the methyl groups is oxidized to alcohol and aldehyde, respectively, which were identified by NMR and ESI-TOF/MS. Such a low oxidation yield of the xylyl linker ($\sim 44\%$) suggests that the amount of intermolecular species is more than 50% under the above conditions. The oxidation of the 6-methyl group is in line with the observation for the decomposition of $[\text{Cu}_2(\text{O}_2)(\text{Me}_2\text{-pybn})_2]^{2+}$ (5-O_2), which also gave a ligand-based alcohol and a ligand-based aldehyde [21]. Thus intermolecular ($\mu\text{-}\eta^2\text{:}\eta^2\text{-peroxo}$) species is capable of oxidation of the 6-methyl group of the supporting ligand.

Decomposition of $[\text{Cu}_2(\text{O}_2)(\text{Me}_2\text{-L-Me})]^{2+}$ (1-O_2 , 0.754 mM) in acetone at -50 °C showed a successive color

change from brown through green to dark-brown. The electronic spectrum of the final dark-brown solution showed an absorption band at 460 nm, reminiscent of formation of a Cu(II) phenolate complex. We have succeeded in the isolation and crystallization of the dark-brown species. Crystal structure revealed that the complex has a dimer structure having $\text{Me}_3\text{-L-O}^-$ ligands, indicating that $\text{Me}_2\text{-L-Me}$ ligand is hydroxylated at the 2-position of the xylyl linker with a 1,2-methyl migration (NIH shift) accompanied by the elimination of a bis(6-methyl-2-pyridylmethyl)aminomethyl sidearm as shown in Fig. 6 and Scheme 3. As noted earlier, a similar observation has already been reported for the oxidation of $[\text{Cu}_2(\text{H-XYL-Me})]^{2+}$ and $[\text{Cu}_2(\text{Me}_2\text{-XYL-Me})]^{2+}$ with dioxygen [4]. Ligand recovery experiment gave $\text{Me}_3\text{-L-OH}$ (yield = $\sim 77\%$ based on 1-O_2) and bis(6-methyl-2-pyridylmethyl)amine ($\text{Me}_2\text{-bpa}$) (yield could not be determined from NMR). Isotope labeling experiment by $^{18}\text{O}_2$ revealed that the oxygen atom of $\text{Me}_3\text{-L-OH}$ comes from $^{18}\text{O}_2$. Occurrence of 1,2-methyl migration indicates that the hydroxylation reaction proceeds via an electrophilic aromatic substitution mechanism involving a carbocationic intermediate [4]. We have also studied decomposition of 2-O_2 in acetone at room temperature. Although ligand recovery experiments showed an original H-L-F and some modified ligands which were detected by NMR and ESI-TOF/MS, it was difficult to identify those modified ligands.

2.4. Kinetic study of decompositions of 1-O_2 , 2-O_2 , and 3-O_2

Decompositions of $[\text{Cu}_2(\text{O}_2)(\text{Me}_2\text{-L-Me})]^{2+}$ (1-O_2) and $[\text{Cu}_2(\text{O}_2)(\text{H-L-F})]^{2+}$ (2-O_2) in acetone (0.1–1.0 mM) obey

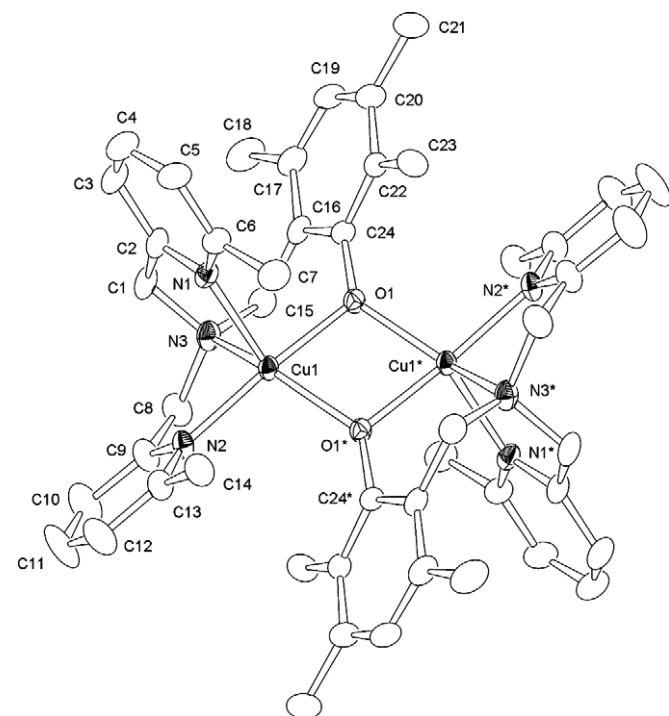
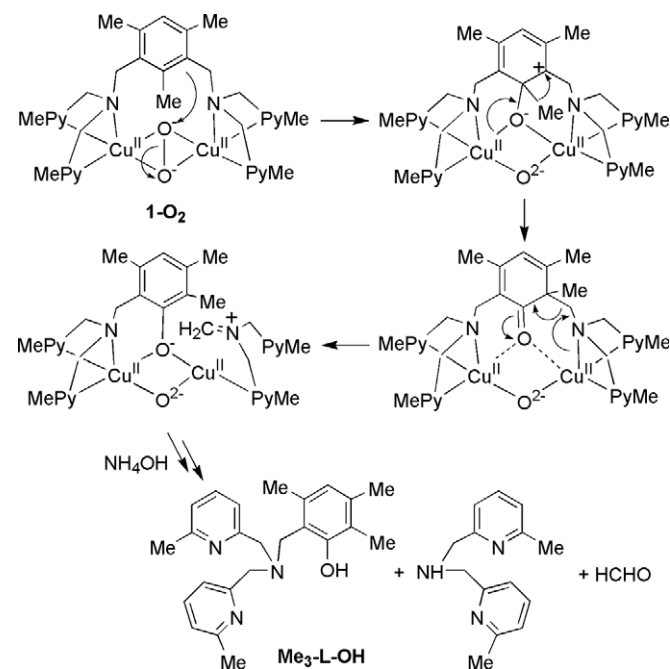


Fig. 6. ORTEP views (50% probability) of the cationic portion of $[\text{Cu}_2(\text{Me}_3\text{-L-O})_2](\text{PF}_6)_2 \cdot \text{C}_2\text{H}_5\text{OH} \cdot \text{H}_2\text{O}$ (**4**). Hydrogen atoms are omitted for clarity. Selected bond distances (Å) and angles (°): Cu1...Cu1* 3.103(1), Cu1-O1 1.952(3), Cu1-O1* 1.989(3), Cu1-N1 2.133(4), Cu1-N2 2.001(4), Cu1-N3 2.091(4), O1-Cu1-O1* 76.1(1), O1-Cu1-N1 91.4(1), O1-Cu1-N2 169.3(1), O1-Cu1-N3 91.7(1), O1*-Cu1-N1 137.1(1), O1*-Cu1-N2 102.8(1), O1*-Cu1-N3 137.4(1), N1-Cu1-N2 96.3(1), N1-Cu1-N3 82.7(1), N2-Cu1-N3 81.9(1).



Scheme 3. A possible oxidation pathway of $[\text{Cu}_2(\text{O}_2)(\text{Me}_2\text{-L-Me})]^{2+}$ (1-O_2) with 1,2-methyl migration (NIH shift).

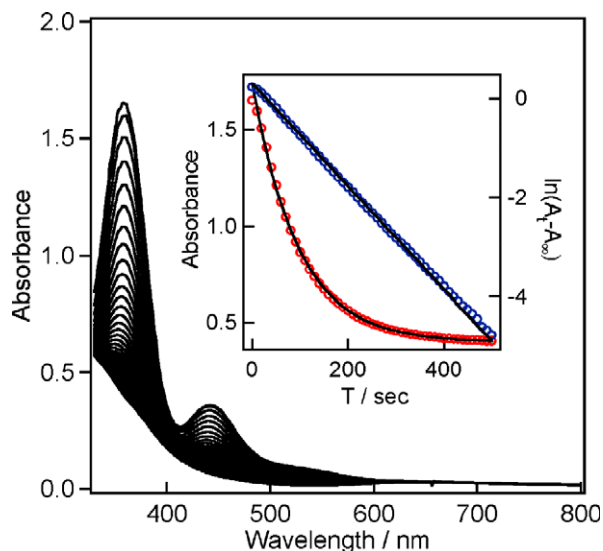


Fig. 7. Representative spectral change for decomposition of **1-O₂** (10 s interval) in acetone at $-50\text{ }^{\circ}\text{C}$. Experimental conditions: $[\mathbf{1-O}_2] = 0.737\text{ mM}$. Inset: Time course of the absorbance change at 359 nm and the first-order kinetic plot.

first-order kinetics (Fig. 7). Comparison of the first order rate constants of **1-O₂** ($1.04 \times 10^{-2}\text{ s}^{-1}$), **2-O₂** ($3.25 \times 10^{-3}\text{ s}^{-1}$), and **3-O₂** ($2.12 \times 10^{-3}\text{ s}^{-1}$) at $-50\text{ }^{\circ}\text{C}$ shown in Table 1 reveals that introduction of fluorine into the xylyl linker has no significant influence on the decomposition rate, but introduction of three methyl groups accelerates the decomposition rate by ~ 5 times. Very recently, we have reported that decomposition rate constants (hydroxylation rate constants of the xylyl linker) of a series of $[\text{Cu}_2(\text{O}_2)(\text{X-L-H})]^{2+}$ ($\text{X-L-H} = \text{H-L-H}$, MeO-L-H , $t\text{-Bu-L-H}$, and $\text{NO}_2\text{-L-H}$) are highly dependent on the electron donating ability of the substituent X and a Hammett ρ value is -1.9 at $-50\text{ }^{\circ}\text{C}$, indicating that the aromatic hydroxylation mediated by $[\text{Cu}_2(\text{O}_2)(\text{X-L-H})]^{2+}$ proceeds via an electrophilic aromatic substitution mechanism. Similar observations have also been made for various complexes such as $[\text{Cu}_2(\text{O}_2)(\text{X-XYL-H})]^{2+}$ ($\rho = -2.1$ at $-80\text{ }^{\circ}\text{C}$) [6b], $[\text{Cu}_2(\text{O}_2)(\text{L}^{\text{py}2\text{Bz}})]^{2+}$ ($\rho = -1.8$) [12], $[\text{Cu}_2(\text{O}_2)(\text{MeL66})]^{2+}$

Table 1
Kinetic parameters for arene hydroxylation by $(\mu\text{-}\eta^2\text{:}\eta^2\text{-peroxo})\text{Cu}(\text{II})_2$ complexes having xylyl linker

Ligand	ΔH^\ddagger (kJ mol ⁻¹)	ΔS^\ddagger (J mol ⁻¹ K ⁻¹)	k_1 (s ⁻¹) ^a	Reference
Me ₂ -L-Me	53 ± 1	-44 ± 6	1.04×10^{-2}	This Work
H-L-F	62 ± 1	-10 ± 6	3.25×10^{-3}	This Work
H-L-H	63 ± 1	-11 ± 1	2.12×10^{-3}	[13]
MeO-L-H	59 ± 1	8 ± 4	1.35×10^{-1}	[13]
<i>t</i> -Bu-L-H	62 ± 1	1 ± 4	1.79×10^{-2}	[13]
NO ₂ -L-H	65 ± 1	-26 ± 3	1.43×10^{-4}	[13]
<i>t</i> -Bu-XYL-H	41 ± 2	-59 ± 8	1.07×10^{-4}	[6]
H-XYL-H	50 ± 1	-35 ± 2	1.49×10^{-1}	[6]
NO ₂ -XYL-H	55 ± 1	-32 ± 2	1.34×10^{-2}	[6]
<i>m</i> -XYL ^{Pr4}	50.1 ± 0.2	-50.4 ± 0.9	1.99×10^{-2}	[7]

^a At $-50\text{ }^{\circ}\text{C}$.

($\rho = -1.84$ at $-55\text{ }^{\circ}\text{C}$) [11], and $[\text{Cu}_2(p\text{-R-PhO})(\text{O})_2(\text{DBED})_2]^{2+}$ ($\rho = -2.2$ at $-120\text{ }^{\circ}\text{C}$) [15]. The rate constant observed for **1-O₂** is in line with the electron donating effect of the methyl groups, which appears to be partly responsible to the decomposition rates of the complex. However, steric effect of the methyl group in the 2-position of the xylyl linker may also contribute to the decomposition rate (vide infra).

Fig. 8 showed Eyring plots for the decompositions of **1-O₂** and **2-O₂**. The activation parameters of **2-O₂** ($\Delta H^\ddagger = 62 \pm 1\text{ kJ mol}^{-1}$ and $\Delta S^\ddagger = -10 \pm 6\text{ J mol}^{-1}\text{ K}^{-1}$) are comparable to those of **3-O₂** ($\Delta H^\ddagger = 63 \pm 1\text{ kJ mol}^{-1}$ and $\Delta S^\ddagger = -11 \pm 3\text{ J mol}^{-1}\text{ K}^{-1}$) as shown in Table 1. Unlike **2-O₂**, the high reactivity of **1-O₂** relative to **3-O₂** is attributable to favorable enthalpy effect (a decrease of the activation enthalpy change, $\Delta H^\ddagger = 53 \pm 1\text{ kJ mol}^{-1}$), although entropy effect is unfavorable (a decrease of the activation entropy change, $\Delta S^\ddagger = -44 \pm 6\text{ J mol}^{-1}\text{ K}^{-1}$). These enthalpy and entropy effects are not in line with a trend attributed to the electronic effect of *p*-substituents X (X = MeO, *t*-Bu, H, and NO₂) observed for a series of $[\text{Cu}_2(\text{O}_2)(\text{X-L-H})]^{2+}$ as seen in Table 1; as the electron donating nature of the substituent X increases, the activation enthalpy changes decrease, but the activation entropy changes increase, suggesting that stereochemical effect of the methyl group in the 2-position of the xylyl linker has a significant influence on a transition state for decomposition.

It should be noted that, although a Hammett ρ value (-2.1 at $-80\text{ }^{\circ}\text{C}$) of a series of $[\text{Cu}_2(\text{O}_2)(\text{X-XYL-H})]^{2+}$ is quite similar to that (-1.9 at $-50\text{ }^{\circ}\text{C}$) of $[\text{Cu}_2(\text{O}_2)(\text{X-L-H})]^{2+}$ complexes, the enthalpy and entropy effects are quite different; for a series of $[\text{Cu}_2(\text{O}_2)(\text{X-XYL-H})]^{2+}$, as the electron donating nature of the substituent X increases, both activation enthalpy and entropy changes decrease.

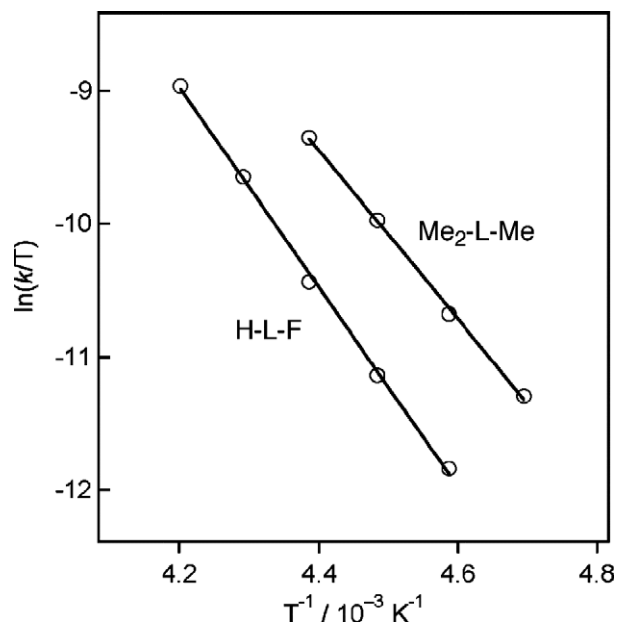


Fig. 8. Eyring plots for the decompositions of **1-O₂** and **2-O₂** in acetone.

Thus, it appears likely that nature of the transition states for decomposition (hydroxylation) of $[\text{Cu}_2(\text{O}_2)(\text{X}-\text{L}-\text{H})]^{2+}$ is different from that of $[\text{Cu}_2(\text{O}_2)(\text{X}-\text{XYL}-\text{H})]^{2+}$.

In summary, we have synthesized dicopper(I) complexes with dinucleating ligands having a xylyl linker, $[\text{Cu}_2(\text{X}-\text{L}-\text{R})]^{2+}$ (**1** and **2**), which generate $(\mu-\eta^2:\eta^2\text{-peroxo})\text{Cu}(\text{II})_2$ species, $[\text{Cu}_2(\text{O}_2)(\text{X}-\text{L}-\text{R})]^{2+}$ (**1-O₂** and **2-O₂**), by the reaction with O_2 in acetone at low temperatures. Resonance Raman and UV–Vis spectroscopies revealed that at low concentrations (less than 5 mM), **1** and **2** produce intramolecular $(\mu-\eta^2:\eta^2\text{-peroxo})\text{Cu}(\text{II})_2$ species, whereas at ~ 60 mM concentration, they form intermolecular $(\mu-\eta^2:\eta^2\text{-peroxo})\text{Cu}(\text{II})_2$ species. Decomposition of **1-O₂** resulted in hydroxylation of the 2-position of the xylyl linker with a NIH shift of the methyl group, suggesting that the hydroxylation proceeds via an electrophilic aromatic substitution mechanism involving a carbocationic intermediate.

3. Experimental

3.1. General

Acetone was dried over Molecular Sieves 4A and distilled under N_2 before use. Bis(6-methyl-2-pyridylmethyl)amine ($\text{Me}_2\text{-bpa}$) [22], 1,3-bis(bromomethyl)-2-fluorobenzene [**4b**], 1,3-bis[bis(6-methyl-2-pyridylmethyl)aminomethyl]benzene (H-L-H) [13] and $[\text{Cu}_2(\text{H-L-H})(\text{PF}_6)_2]$ [13] were synthesized according to the literature methods. All other reagents and solvents were commercially available and used without further purification.

3.2. Syntheses of ligands

1,3-Bis[bis(6-methyl-2-pyridylmethyl)aminomethyl]-2,4,6-trimethylbenzene ($\text{Me}_2\text{-L-Me}$). To a mixture of bis(6-methyl-2-pyridylmethyl)amine (4.72 g, 20.8 mmol) and 2,4-bis(chloromethyl)-1,3,5-trimethylbenzene (2.25 g, 10.4 mmol) in chloroform (100 mL) was added an aqueous solution (30 mL) of $\text{Na}_2\text{CO}_3 \cdot \text{H}_2\text{O}$ (2.58 g, 20.8 mmol). Reaction mixture was vigorously stirred at room temperature for 3 days. The mixture was extracted with chloroform ($3 \times 30 \text{ cm}^3$) and the combined extracts were dried over Na_2SO_4 and evaporated under reduced pressure to give an orange oil, which was dissolved into hot hexane (200 mL) and insoluble material was removed by decantation. The resulting hexane solution was allowed to stand at -80°C to give a yellow oil, which was isolated and dissolved into 20 mL of ethanol. The solution was allowed to stand for a week to yield a yellow powder. Yield: 4.46 g (72 %). ^1H NMR (CDCl_3 , 400 MHz): δ (ppm) = 7.46 (t, 4H, pyH), 7.21 (d, 4H, pyH), 6.95 (d, 4H, pyH), 6.71 (s, 1H, xylH), 3.70 (s, 12H, $\text{NCH}_2\text{py} + \text{NCH}_2\text{xyl}$), 2.50 (s, 12H, pyCH_3), 2.29 (s, 3H, xyl CH_3), 2.22 (s, 6H, xyl CH_3). $^{13}\text{C}\{^1\text{H}\}$ NMR (CDCl_3 , 100.4 MHz): δ (ppm) = 159.4 (py), 157.0 (py), 138.9 (xyl), 137.0 (xyl), 136.2 (py), 132.8 (xyl), 130.0 (xyl), 121.1 (py),

120.0 (py), 60.2 (CH_2), 52.8 (CH_2), 24.3 (pyCH_3), 20.4 (xyl CH_3), 16.1 (xyl CH_3). ESI-TOF/MS (acetonitrile solution containing a small amount of formic acid): m/z (relative intensity) = 300.19 (100) $[\text{M} + 2\text{H}]^{2+}$, 599.39 (3) $[\text{M} + \text{H}]^+$. Anal. Calc. for $\text{C}_{39}\text{H}_{46}\text{N}_6$: C, 78.22; H, 7.74; N, 14.03. Found: C, 78.04; H, 7.84; N, 13.90%.

1,3-Bis[bis(6-methyl-2-pyridylmethyl)aminomethyl]-2-fluorobenzene $\cdot 0.5\text{H}_2\text{O}$ (H-L-F). To a mixture of bis(6-methyl-2-pyridylmethyl)amine (5.45 g, 24.0 mmol) and 1,3-bis(bromomethyl)-2-fluorobenzene (3.39 g, 12.0 mmol) in chloroform (100 mL) was added an aqueous solution (30 mL) of $\text{Na}_2\text{CO}_3 \cdot \text{H}_2\text{O}$ (2.98 g, 24.0 mmol). The reaction mixture was vigorously stirred at room temperature for three days. The mixture was extracted with chloroform ($3 \times 30 \text{ cm}^3$) and the combined extracts were dried over Na_2SO_4 and evaporated under reduced pressure to give an orange oil, which was dissolved into hot hexane (200 mL) and insoluble material was removed by decantation. The resulting hexane solution was allowed to stand at -80°C to give a white powder. Yield: 6.53 g (93%). ^1H NMR ($(\text{CD}_3)_2\text{CO}$, 400 MHz): δ (ppm) = 7.59 (4H, t, pyH), 7.54 (2H, t, xylH), 7.43 (4H, d, pyH), 7.13 (1H, t, xylH), 7.05 (4H, d, pyH), 3.76 (12H, s, $\text{NCH}_2\text{py} + \text{NCH}_2\text{xyl}$), 2.44 (12H, s, pyCH_3). $^{13}\text{C}\{^1\text{H}\}$ NMR (CDCl_3 , 100.4 MHz): δ (ppm) = 160.0 (d, xylC-F), 159.2 (py), 157.4 (py), 136.6 (py), 129.8 (xyl), 125.7 (xyl), 123.4 (xyl), 121.3 (py), 119.3 (py), 60.3 (CH_2), 51.6 (CH_2), 24.4 (pyCH_3). ESI-TOF/MS (acetonitrile solution containing a small amount of formic acid): m/z (relative intensity) = 288.17 (100) $[\text{M} + 2\text{H}]^{2+}$, 575.34 (4) $[\text{M} + \text{H}]^+$. Anal. Calc. for $\text{C}_{36}\text{H}_{40}\text{N}_6\text{O}_{0.5}\text{F}_1$: C, 74.07; H, 6.91; N, 14.40. Found: C, 74.06; H, 6.84; N, 14.48%.

3.3. Syntheses of complexes

Copper(I) complexes were prepared under N_2 atmosphere using standard Schlenk techniques. *Caution: All the perchlorate salts are potentially explosive and should be handled with care.*

$[\text{Cu}_2(\text{Me}_2\text{-L-Me})(\text{CH}_3\text{CN})_2](\text{PF}_6)_2 \cdot \text{H}_2\text{O}$ (**1-CH₃CN**). Using the same procedure as described for the synthesis of $[\text{Cu}_2(\text{H-L-H})(\text{CH}_3\text{CN})_2](\text{PF}_6)_2$ [13], an ethanol suspension (10 mL) containing $[\text{Cu}(\text{CH}_3\text{CN})_4]\text{ClO}_4$ (0.327 g, 1.00 mmol), $\text{Me}_2\text{-L-Me}$ (0.308 g, 0.514 mmol), and NH_4PF_6 (0.330 g, 2.03 mmol) was heated to give a yellow solution, which was allowed to stand for a day to afford a yellow–green powder. Yield: 0.425 g (76 %). ^1H NMR ($(\text{CD}_3)_2\text{CO}$, 300 MHz): δ (ppm) = 7.83 (4H, t, pyH), 7.43 (4H, d, pyH), 7.33 (4H, d, pyH), 6.93 (1H, s, xylH), 4.06 (4H, s, NCH_2xyl), 3.99 (8H, s, NCH_2py), 2.77 (12H, s, pyCH_3), 2.43 (3H, s, xyl CH_3), 2.32 (6H, s, xyl CH_3), 2.23 (6H, s, CH_3CN). FTIR (KBr, cm^{-1}): 1604 (C=C, aromatic), 1577 (C=C, aromatic), 847 (PF_6^-), 557 (PF_6^-). ESI-TOF/MS (acetonitrile under N_2 atmosphere): m/z (relative intensity) = 362.12 (100) $[\text{Cu}_2(\text{Me}_2\text{-L-Me})]^{2+}$. Anal. Calc. for $\text{C}_{43}\text{H}_{54}\text{N}_8\text{O}_1\text{Cu}_2\text{F}_{12}\text{P}_2$: C, 46.28; H, 4.88; N, 10.04. Found: C, 46.03; H, 4.73; N, 9.96%. Recrystallization

of **1**-CH₃CN from EtOH/H₂O/CH₃CN mixture gave single crystals, [Cu₂(Me₂-L-Me)(CH₃CN)₂](PF₆)₂ · 0.5CH₃CN · 0.25H₂O (**1a**-CH₃CN), suitable for X-ray crystallography.

[Cu₂(Me₂-L-Me)(CO)₂](PF₆)₂ (**1**-CO). This was synthesized as a white powder in the same manner as described for synthesis of [Cu₂(H-L-H)(CO)₂](PF₆)₂ [13] using [Cu₂(Me₂-L-Me)(CH₃CN)₂](PF₆)₂ · H₂O (0.425 g, 0.381 mmol). Yield: 0.376 g (92 %). ¹H NMR ((CD₃)₂CO, 400 MHz): δ (ppm) = 7.94 (4H, t, pyH), 7.52 (4H, d, pyH), 7.46 (4H, d, pyH), 7.11 (1H, s, xylH), 3.75–4.32 (12H, m, NCH₂py + NCH₂xyl), 2.81 (12H, s, pyCH₃), 2.59 (3H, s, xylCH₃), 2.33 (6H, s, xylCH₃). FTIR (KBr, cm⁻¹): 2096 (C≡O), 2085 (C≡O), 1606 (C=C, aromatic), 1577 (C=C, aromatic), 837 (PF₆⁻), 557 (PF₆⁻). ESI-TOF/MS (acetone under N₂ atmosphere): *m/z* (relative intensity) = 362.12 (100) [Cu₂(Me₂-L-Me)]²⁺, 376.12 (16) [Cu₂(Me₂-L-Me)(CO)]²⁺. Anal. Calc. for C₄₁H₄₆N₆O₂ · Cu₂F₁₂P₂: C, 45.94; H, 4.33; N, 7.84. Found: C, 46.15; H, 4.34; N, 7.91%.

[Cu₂(Me₂-L-Me)](PF₆)₂ (**1**). This was prepared by the same method as described for synthesis of [Cu₂(H-L-H)](PF₆)₂ [13] except [Cu₂(Me₂-L-Me)(CO)₂](PF₆)₂ was used. ESI-TOF/MS (acetone under N₂ atmosphere): *m/z* (relative intensity) = 362.12 (100) [Cu₂(Me₂-L-Me)]²⁺. FTIR (KBr, cm⁻¹): 1610 (C=C, aromatic), 1576 (C=C, aromatic), 839 (PF₆⁻), 557 (PF₆⁻).

[Cu₂(H-L-F)(CH₃CN)₂](PF₆)₂ (**2**-CH₃CN). The complex was prepared by the method similar to the synthesis of [Cu₂(H-L-H)(CH₃CN)₂](PF₆)₂ [13]. An ethanol suspension (10 mL) containing [Cu(CH₃CN)₄]ClO₄ (0.327 g, 1.00 mmol), H-L-F · 0.5H₂O (0.292 g, 0.500 mmol), and NH₄PF₆ (0.325 g, 1.99 mmol) was heated to give a yellow solution, which was allowed to stand for a day to afford a yellow–green powder. Yield: 0.489 g (91%). ¹H NMR ((CD₃)₂CO, 400 MHz): δ (ppm) = 7.84 (4H, t, pyH), 7.56 (2H, t, xylH), 7.43 (4H, d, pyH), 7.33 (4H, d, pyH), 7.22 (1H, t, xylH), 3.82–4.17 (12H, m, NCH₂py + NCH₂xyl), 2.79 (12H, s, pyCH₃), 2.34 (6H, s, CH₃CN). FTIR (KBr, cm⁻¹): 1604 (C=C, aromatic), 1577 (C=C, aromatic), 850 (PF₆⁻), 557 (PF₆⁻). ESI-TOF/MS (acetone under N₂ atmosphere): *m/z* (relative intensity) = 350.09 (100) [Cu₂(H-L-F)]²⁺, 370.61 (34) [Cu₂(H-L-F)(CH₃CN)]²⁺, 391.12 (2) [Cu₂(H-L-F)(CH₃CN)₂]²⁺. Anal. Calc. for C₄₀H₄₅N₈Cu₂F₁₃P₂: C, 44.74; H, 4.22; N, 10.43. Found: C, 44.62; H, 4.24; N, 10.55%.

[Cu₂(H-L-F)(CO)₂](PF₆)₂ (**2**-CO). This was synthesized as a white powder in the same manner as described for synthesis of [Cu₂(H-L-H)(CO)₂](PF₆)₂ [13] using [Cu₂(H-L-F)(CH₃CN)₂](PF₆)₂ (0.489 g, 0.455 mmol). Yield: 0.447 g (94%). ¹H NMR ((CD₃)₂CO, 400 MHz): δ (ppm) = 7.90 (4H, t, pyH), 7.67 (2H, t, xylH), 7.49 (4H, d, pyH), 7.39 (4H, d, pyH), 7.26 (1H, t, xylH), 4.43 (4H, d, NCH₂py), 4.39 (4H, s, NCH₂xyl), 4.00 (4H, d, NCH₂py), 2.82–2.85 (12H, m, pyCH₃). FTIR (KBr, cm⁻¹): 2089 (C≡O), 1608 (C=C, aromatic), 1577 (C=C, aromatic), 839 (PF₆⁻), 557 (PF₆⁻). ESI-TOF/MS (acetone under N₂ atmosphere): *m/z* (relative intensity) = 350.09 (100) [Cu₂(H-L-F)]²⁺,

364.09 (12) [Cu₂(H-L-F)(CO)]²⁺. Anal. Calc. for C₃₈H₃₉N₆O₂Cu₂F₁₃O₂P₂: C, 43.55; H, 3.75; N, 8.02. Found: C, 43.87; H, 3.77; N, 8.10%.

[Cu₂(H-L-F)](PF₆)₂ (**2**). This was prepared by the same method as described for synthesis of [Cu₂(H-L-H)](PF₆)₂ [13] except [Cu₂(H-L-F)(CO)₂](PF₆)₂ was used. ESI-TOF/MS (acetone under N₂ atmosphere): *m/z* (relative intensity) = 350.09 (100) [Cu₂(H-L-F)]²⁺. FTIR (KBr, cm⁻¹): 1610 (C=C, aromatic), 1576 (C=C, aromatic), 843 (PF₆⁻), 559 (PF₆⁻).

[Cu₂(Me₃-L-O)₂](PF₆)₂ · C₂H₅OH · H₂O (**4**). [Cu₂(Me₂-L-Me)](PF₆)₂ (0.0250 mmol) prepared from [Cu₂(Me₂-L-Me)(CO)₂](PF₆)₂ (0.0268 g, 0.0250 mmol) was dissolved in acetone (10 mL). The solution was then exposed to O₂ at room temperature to give a dark-brown solution, to which was added 5 mL of ethanol. The solution was allowed to stand for a week to yield dark brown crystals suitable for X-ray analysis. Yield: 0.0200 g (65 %). FTIR (KBr, cm⁻¹): 1608 (C=C, aromatic), 1577 (C=C, aromatic), 837 (PF₆⁻), 557 (PF₆⁻). UV-Vis (acetonitrile, 0.132 mM) (λ_{max}/nm (ε/M⁻¹ cm⁻¹)): 460 (6300), 330 (4200, sh). Anal. Calc. for C₅₀H₆₄N₆Cu₂F₁₂O₄P₂: C, 48.82; H, 5.24; N, 6.83. Found: C, 48.73; H, 5.33; N, 6.69%. ESI-TOF/MS (acetonitrile): *m/z* (relative intensity) = 437.15 (100) [Cu₂(Me₃-L-O)]²⁺.

3.4. Physical measurements

The electronic spectra were measured with a Shimadzu diode array spectrometer Multispec-1500 with a Unisoku thermostated cell holder designed for low-temperature experiments.

Resonance Raman spectra were obtained with a liquid nitrogen cooled CCD detector (LN/CCD-1100-PB, Roper Scientific) attached to a 1 m-single polychromator (Model MC-100DG, Ritsu Oyo Kogaku). The 406.7 nm line of a Kr⁺ laser (Model 2060 Spectra Physics) and 514.5 nm line of an Ar⁺ laser (GLC 3200, NEC) were used as the exciting sources. The laser powers used for the 406.7 and 514.5 nm excitations were 2 and 10 mW, respectively, at the sample points. All measurements were carried out with a spinning cell (1000 rpm) keeping at -80 to -90 °C. Raman shifts were calibrated with indene and the accuracy of the peak positions of the Raman bands was ±1 cm⁻¹.

¹H and ¹³C{¹H} NMR spectra were measured with JEOL JNM-LM300 or -LM400 using tetramethylsilane (TMS) for ¹H NMR and *d*₁-chloroform for ¹³C{¹H} NMR as the internal standards. Infrared spectra were obtained by KBr disk method with a HORIBA FT-200 spectrophotometer.

3.5. Isolation and identification of modified ligands by thermal decomposition of [Cu₂(O)₂(H-L-H)](PF₆)₂ (3-O₂) under O₂

Ligand recovery experiment was performed as follows. Typically, **3** (0.0605 mmol) prepared from **3**-CO

(0.0623 g, 0.0605 mmol) was dissolved into 1 mL of acetone and the resulting solution (60.5 mM) was exposed to O₂ at –78 °C and allowed to stand at –60 °C overnight to complete the decomposition. Evaporation of acetone under reduced pressure yielded a dark green oil. To this oil was added CHCl₃ (20 mL) and concentrated aqueous ammonia (20 mL) with stirring. Organic compounds were extracted with CHCl₃ (3 × 20 mL). The combined extracts were dried over Na₂SO₄ and chloroform was removed by evaporation under a reduced pressure to give an oil. H–L–OH, H–L–H and the modified ligands in which one of 6-methyl group of pyridyl group is oxidized to alcohol and aldehyde which were identified by ¹H NMR and ESI-TOF/MS, and their amounts were determined by ¹H NMR by addition of 1 mL of 2,6-dimethyl-1,4-benzoquinone CDCl₃ solution (0.0256 M) as an internal standard. Yield of H–L–H, H–L–OH, ligand-based alcohol, and ligand-based aldehyde were 38, 44, 7, and 9% based on **3-CO**, respectively. H–L–OH: ¹H NMR (CDCl₃, 300 MHz): δ (ppm) = 7.49 (4H, t, pyH), 7.33 (4H, d, pyH), 7.20 (2H, d, xylH), 6.97 (4H, d, pyH), 6.74 (1H, t, xylH), 3.83 (8H, s, NCH₂py), 3.79 (4H, s, NCH₂xyl), 2.52 (12H, s, pyCH₃). ESI-TOF/MS (acetonitrile solution containing a small amount of formic acid): *m/z* (relative intensity) = 287.17 (100) [M + 2H]²⁺, 573.33 (24), [M + H]⁺.

3.6. Isolation and identification of modified ligands by thermal decomposition of [Cu₂(O)₂(Me₂–L–Me)](PF₆)₂ (1-O₂) under O₂

Ligand recovery experiment was performed as follows. Typically, **1** (0.0188 mmol) prepared from **1-CO** (0.0202 g, 0.0188 mmol) was dissolved into 25 mL of acetone and the resulting solution (0.754 mM) was exposed to O₂ at –50 °C and allowed to stand one hour to complete the decomposition. Evaporation of acetone under reduced pressure yielded a dark brown oil. To this oil was added CHCl₃ (20 mL) and concentrated aqueous ammonia (20 mL) containing excess Na₄EDTA with vigorously stirring. Organic compounds were extracted with CHCl₃ (3 × 20 mL). The combined extracts were dried over Na₂SO₄ and chloroform was removed by evaporation under a reduced pressure to give an oil. The reaction products were identified by ¹H NMR and ESI-TOF/MS, and their amounts were determined by ¹H NMR by addition of 1 mL of 2,6-dimethyl-1,4-benzoquinone CDCl₃ solution (0.0190 M) as an internal standard. Yield of Me₃–L–OH was 77 % based on **1-CO**. Me₃–L–OH: ¹H NMR (CDCl₃, 400 MHz): δ (ppm) = 7.53 (2H, t, pyH), 7.20 (2H, d, pyH), 7.01 (2H, d, pyH), 6.46 (1H, s, xylH), 3.81 (6H, s, NCH₂py + NCH₂xyl), 2.56 (6H, s, pyCH₃), 2.21 (3H, s, xylCH₃), 2.18 (3H, s, xylCH₃), 2.15 (3H, s, xylCH₃). ESI-TOF/MS (acetonitrile solution containing a small amount of formic acid): *m/z* (relative intensity) = 376.24 (100) [M + H]⁺.

3.7. Kinetic measurements

The decompositions of [Cu₂(O₂)(Me₂–L–Me)]²⁺ (**1-O₂**) and [Cu₂(O₂)(L–F)]²⁺ (**2-O₂**) were followed in 1 mm path length UV–Vis cell that was held in a Unisoku thermostated cell holder designed for low temperature experiments. Acetone solutions of **1-O₂** (0.2–1.0 mM) and **2-O₂** (0.1–0.5 mM) were kept at the desired temperatures for 30 min, O₂ gas was bubbled for 5–10 s. Rate constants for decompositions of **1-O₂** and **2-O₂** were determined by monitoring decrease of the absorbance at 359 and 353 nm, respectively.

3.8. ¹⁸O₂ labeling experiments

Hydroxylation of ligand was also performed using ¹⁸O₂. The procedures were the same as those of ¹⁶O₂ experiments except for using ¹⁸O₂. Me₃–L–¹⁸OH: ESI-TOF/MS (acetonitrile solution containing a small amount of formic acid): *m/z* (relative intensity) = 378.25 (100) [Me₃–L–¹⁸OH + H]⁺. Me₃–L–¹⁶OH: ESI-TOF/MS (acetonitrile solution containing a small amount of formic acid): *m/z* (relative intensity) = 376.24 (100) [Me₃–L–¹⁶OH + H]⁺.

Table 2

Crystallographic data for [Cu₂(Me₂–L–Me)(CH₃CN)₂](PF₆)₂ · 0.5CH₃CN · 0.25H₂O (**1a-CH₃CN**), and [Cu₂(Me₃–L–O)₂](PF₆)₂ · C₂H₅OH · H₂O (**4**)

	1a-CH₃CN	4
Empirical formula	C ₄₄ H ₅₄ O _{0.25} N _{8.5} Cu ₂ P ₂ F ₁₂	C ₅₀ H ₆₄ O ₄ N ₆ Cu ₂ P ₂ F ₁₂
Formula weight	1122.99	1230.11
Crystal system	Monoclinic	Triclinic
Space group	P2 ₁ /c (#14)	P $\bar{1}$ (#2)
Unit cell dimension		
<i>a</i> (Å)	23.111(2)	9.446(2)
<i>b</i> (Å)	8.6299(9)	12.033(2)
<i>c</i> (Å)	27.442(2)	13.149(2)
α (°)	90	73.65(1)
β (°)	112.972(2)	65.24(1)
γ (°)	90	86.27(1)
<i>V</i> (Å ³)	5039.1(6)	1299.9(4)
<i>Z</i>	4	1
2 θ _{max}	60.9	55.0
<i>F</i> (000)	2302.00	634.00
<i>D</i> _{calc} (g cm ⁻³)	1.480	1.571
μ (Mo K α) (cm ⁻¹)	9.93	9.74
Temperature (°C)	–155	–150
Number of measured reflections	29443	13456
Number of unique reflections	6534 (<i>I</i> ≥ 3.00σ(<i>I</i>))	4461 (<i>I</i> ≥ 3.00σ(<i>I</i>))
Number of variables	620	347
Goodness-of-fit	1.45	1.69
Maximum and minimum of residual electron density (e Å ⁻³)	1.38 and –0.62	1.85 and –0.85
<i>R</i> ^a	0.056	0.068
<i>wR</i> ^b	0.088	0.100

^a $R = \sum ||F_o| - |F_c|| / \sum |F_o|$ (*I* ≥ 3.0σ(*I*)).

^b $wR = [\sum w(|F_o| - |F_c|)^2 / \sum w|F_o|^2]^{1/2}$; $w = 1/[\sigma^2(F_o) + p^2|F_o|^2/4]$ (*p* = 0.079 for **1a-CH₃CN** and *p* = 0.098 for **4**).

3.9. X-ray crystallography. General procedures

Data collections were carried out on a Rigaku/MSM Mercury diffractometer with graphite monochromated Mo K α radiation ($\lambda = 0.71070$ Å). All the structures were solved and refined by the teXsan crystallographic software package [23]. Lorentz and polarization corrections were applied to the data. Empirical absorption corrections (multi-scan) were also applied. The structures were solved by direct methods using SIR92 [24] for **1a**-CH₃CN and SHELXS86 [25] for **4**, and expanded using DIRDIF-94 [26]. The space groups were confirmed by the systematic absences, and the successful solution and refinements of the structures. Crystallographic data are summarized in Table 2. Crystallographic data have been deposited with the Cambridge Crystallographic Data Center as supplemental publication no. CCDC 600563-600564. Copies of this information may be obtained free of charge from The Director, CCDC, 12 Union Road, Cambridge, CB2 1EZ, UK (fax: +44-1223-336-033; e-mail: deposit@ccdc.cam.ac.uk or www: <http://www.ccdc.cam.ac.uk>).

Acknowledgement

This work was supported by Grants-in-Aid for Scientific Research (KAKENHI) on Priority Areas “Dynamic Complex” from the Ministry of Education, Science, and Culture, Japan.

Appendix A. Supplementary data

Supplementary data associated with this article can be found, in the online version, at [doi:10.1016/j.jorganchem.2006.05.068](https://doi.org/10.1016/j.jorganchem.2006.05.068).

References

- [1] (a) K.D. Karlin, A.D. Zuberbühler, in: J. Reedijk, E. Bouwman (Eds.), *Bioinorganic Catalysis*, 2nd ed., Marcel Dekker, New York, 1999, pp. 469–534;
- (b) E.I. Solomon, P. Chen, M. Metz, S.-K. Lee, A.E. Palmer, *Angew. Chem., Int. Ed.* 40 (2001) 4570;
- (c) S. Itoh, S. Fukuzumi, *Bull. Chem. Soc. Jpn.* 75 (2002) 2081;
- (d) E.A. Lewis, W.B. Tolman, *Chem. Rev.* 104 (2004) 1047;
- (e) L.M. Mirica, X. Ottenwaelder, T.D.P. Stack, *Chem. Rev.* 104 (2004) 1013;
- (f) L.Q. Hatcher, K.D. Karlin, *J. Biol. Inorg. Chem.* 9 (2004) 669.
- [2] Y. Matoba, T. Kumagai, A. Yamamoto, H. Yoshitsu, M. Sugiyama, *J. Biol. Chem.* 281 (2006) 8981.
- [3] (a) K.D. Karlin, Y. Gultneh, J.P. Hutchinson, J. Zubieta, *J. Am. Chem. Soc.* 104 (1982) 5240;
- (b) K.D. Karlin, J.C. Hayes, Y. Gultneh, R.W. Cruse, J.W. McKown, J.P. Hutchinson, J. Zubieta, *J. Am. Chem. Soc.* 106 (1984) 2121.
- [4] (a) K.D. Karlin, B.I. Cohen, R.R. Jacobson, J. Zubieta, *J. Am. Chem. Soc.* 109 (1987) 6194;
- (b) M.S. Nasir, B.I. Cohen, K.D. Karlin, *J. Am. Chem. Soc.* 114 (1992) 2482.
- [5] E. Pidcock, H.V. Obias, C.X. Zhang, K.D. Karlin, E.I. Solomon, *J. Am. Chem. Soc.* 120 (1998) 7841.
- [6] (a) R.W. Cruse, S. Kaderli, K.D. Karlin, A.D. Zuberbühler, *J. Am. Chem. Soc.* 110 (1988) 6882;
- (b) K.D. Karlin, M.S. Nasir, B.I. Cohen, R.W. Cruse, S. Kaderli, A.D. Zuberbühler, *J. Am. Chem. Soc.* 116 (1994) 1324.
- [7] S. Mahapatra, S. Kaderli, A. Llobet, Y.-M. Neuhold, T. Palanché, J.A. Halfen, V.G. Young Jr., T.A. Kaden, L. Que Jr., A.D. Zuberbühler, *W.B. Tolman, Inorg. Chem.* 36 (1997) 6343.
- [8] L. Santagostini, M. Gullotti, E. Monzani, L. Casella, R. Dillinger, F. Tucek, *Chem. Eur. J.* 6 (2000) 519.
- [9] S. Itoh, H. Kumei, M. Taki, S. Nagatomo, T. Kitagawa, S. Fukuzumi, *J. Am. Chem. Soc.* 123 (2001) 6708.
- [10] L.M. Mirica, M. Vance, D.J. Rudd, B. Hedman, K.O. Hodgson, E.I. Solomon, T.D.P. Stack, *J. Am. Chem. Soc.* 124 (2002) 9332.
- [11] S. Palavicini, A. Granata, E. Monzani, L. Casella, *J. Am. Chem. Soc.* 127 (2005) 18031.
- [12] S. Yamazaki, S. Itoh, *J. Am. Chem. Soc.* 125 (2003) 13034.
- [13] T. Matsumoto, H. Furutachi, M. Kobino, M. Tomii, S. Nagatomo, T. Toshi, T. Osako, S. Fujinami, S. Itoh, T. Kitagawa, M. Suzuki, *J. Am. Chem. Soc.* 128 (2006) 3874.
- [14] P.L. Holland, K.R. Rodgers, W.B. Tolman, *Angew. Chem., Int. Ed.* 38 (1999) 1139.
- [15] L.M. Mirica, M. Vance, D.J. Rudd, B. Hedman, K.O. Hodgson, E.I. Solomon, T.D.P. Stack, *Science* 308 (2005) 1890.
- [16] T. Osako, S. Terada, T. Toshi, S. Nagatomo, H. Furutachi, S. Fujinami, T. Kitagawa, M. Suzuki, S. Itoh, *J. Chem. Soc. Dalton* (2005) 3514.
- [17] S. Mahapatra, J.A. Halfen, E.C. Wilkinson, G. Pan, X. Wang, V.G. Young Jr., C.J. Cramer, L. Que Jr., W.B. Tolman, *J. Am. Chem. Soc.* 118 (1996) 11555.
- [18] M.J. Henson, P. Mukherjee, D.E. Root, T.D.P. Stack, E.I. Solomon, *J. Am. Chem. Soc.* 121 (1999) 10332.
- [19] P.L. Holland, C.J. Cramer, E.C. Wilkinson, S. Mahapatra, K.R. Rodgers, S. Itoh, M. Taki, S. Fukuzumi, L. Que Jr., W.B. Tolman, *J. Am. Chem. Soc.* 122 (2000) 792.
- [20] E. Pidcock, H.V. Obias, M. Abe, H.-C. Liang, K.D. Karlin, E.I. Solomon, *J. Am. Chem. Soc.* 121 (1999) 1299.
- [21] S. Terada, M. Suzuki, et al. Unpublished data.
- [22] H. Nagano, N. Komeda, M. Mukaida, M. Suzuki, K. Tanaka, *Inorg. Chem.* 35 (1996) 6809.
- [23] teXsan: Crystal Structure Analysis Package, Molecular Structure Corporation: The Woodlands, TX, 1985 and 1992.
- [24] SIR-92: A. Altomare, G. Casciarano, C. Giacovazzo, A. Guagliardi, M.C. Burla, G. Polidori, M. Camalli, *J. Appl. Crystallogr.* 27 (1994) 435.
- [25] G.M. Sheldrick, in: G.M. Sheldrick, C. Kruger, R. Goddard (Eds.), *Crystallographic Computing 3*, Oxford University Press, 1985, pp. 175–189.
- [26] P.T. Beurskens, G. Admiraal, G. Beurskens, W.P. Bosman, R. de Gelder, R. Israel, J.M.M. Smits, The DIRDIF-94 program system, Technical Report of the Crystallography Laboratory, University of Nijmegen, The Netherlands, 1994.